Accurate ab Initio Calculations on the Rate Constants of the Direct Hydrogen Abstraction Reaction $C_2H + H_2 \rightarrow C_2H_2 + H$

Xiang Zhang,* Yi-hong Ding, Ze-sheng Li, Xu-ri Huang, and Chia-chung Sun

State Key Laboratory of Theoretical and Computational Chemistry, Institute of Theoretical Chemistry, Jilin University, Changchun, Jilin 130023, People's Republic of China

Received: April 4, 2000; In Final Form: June 29, 2000

The direct hydrogen abstraction process for the reaction $C_2H + H_2 \rightarrow C_2H_2 + H$ is theoretically investigated at the UQCISD/6-311+G(d,p) and G2//UQCISD levels. The reaction rate constants over a wide range of temperatures from 20−5000 K are calculated over a wide range of temperatures from 20−5000 K using the canonical variational transition state theory along with the small curvature tunneling correction. At the G2//UQCISD level without and with zero-point vibrational correction, the obtained forward reaction barrier are 2.22 and 2.52 kcal/mol, respectively, which, for the first time, well match the value 2.0−2.5 kcal/mol expected by many groups. The obtained forward rate constants are also in good agreement with most of the available experimental results covering a wide temperature range. Furthermore, the calculated reverse rate constants agree well with two recent experimental estimates yet differ from the other experimental estimates and one ab initio calculation at lower level. Finally, our calculated results show that for the forward reaction, the variational effect should be considered at high temperatures whereas the tunneling correction is very important at the temperatures below 500 K and is much more remarkable below 150 K. For the reverse reaction within the considered temperature range 800−5000 K, the variational effect should also be included in the calculation of rate constants at high temperatures while the small-curvature tunneling correction is small.

1. Introduction

The ethynyl radical C_2H is of fundamental importance in a number of chemical systems. It has been detected as one of the most abundant species in interstellar space[1] and in planetary atmosphere.[2] It is also recognized as an important intermediate in fuel-rich hydrocarbon combustion processes[3] and as a dominant chain carrier during the pyrolysis of acetylene at temperatures in excess of 1800 K.[4,5] To understand the kinetic properties of the ethynyl radical in diverse environments, it is very important to know the rate coefficients of the reactions of C_2H. A number of experiments have been carried out to measure the rate constants of the C_2H reactions with H_2 and CH_4, C_2H_2 and other small species.[6−27] Also, there have been several theoretical work on the rate constants and potential energy surface feature of the C_2H reactions with H_2, O_2 and NO.[28−33]

Among the C_2H reactions, the title reaction $C_2H + H_2 \rightarrow C_2H_2 + H$ is the simplest and has also been the most extensively studied. Up to now, the rate constants of this reaction have been measured over broad temperature ranges from 178 to 854 K and 2580 to 4650 K with most data at room temperature.[6−9,11−13,15,17,19,22,24,26] Theoretically, ab initio calculations of this reaction have been carried out by Harding et al.[28] at SOGVB, SOGVB−CI and POL-CI levels with DZP basis set and by Kamiya[29] at MP2/6-31G(d,p) level. A linear transition state was located in both calculations and the barrier heights were computed to be 4.0 kcal/mol at the POL-CI level[28] and 4.76 kcal/mol at the MP2/6-31G(d,p) level.[29] It has been agreed upon[17,18,24,30] that, instead of the calculated barrier heights, the artificially adjusted value between 2 and 2.5 kcal/mol might better fit the experimental data over a wide temperature range. The potential energy surfaces obtained by Harding et al.[28] and Kamiya[29] were further made use of to perform other theoretical treatments[17,18,24,30,31] on this reaction including the statistical phase space theory by Herbst[30] to evaluate the tunneling effect at low temperatures from 10 to 300 K and the reduced dimensionality quantum calculations by Wang et al.[31] to explore the unusual mode specificity within the reaction.

It seems that further theoretical investigation on the title reaction at higher levels than previously used is still very desirable. First, the barrier heights calculated by Harding et al.[28] and Kamiya[29] were significantly higher than the value 2.0−2.5 kcal/mol expected by many groups.[17,18,24,28,30] Thus, the present ab initio study attempts to reproduce this long expected value. Second, this study serves to predict the rate constants for the low temperatures down to 20 K since the experimental data at very low temperatures are still not available presently despite the potential importance of this reaction in interstellar space. Finally, our study aims to provide an accurate potential energy surface as a useful basis for future other theoretical treatments such as statistical phase space theory and quantum calculations. Actually, Herbst[30] has claimed that his statistical phase space model for calculating the rate coefficients for the title reaction at low temperature is highly sensitive to the transition state barrier and the imaginary frequency of vibration.

Another objective of the present paper is to study the rate constants of the reverse hydrogen abstraction reaction $C_2H_2 + H \rightarrow C_2H + H_2$. This reaction has been believed to play a significant role in the oxidation, photolysis, and pyrolysis of hydrocarbon compounds at high temperature. Both experimental[34−38] and theoretical[31,39] rate constants have been reported. However, these experimental investigations are indirect and we note that some distinct discrepancies still exist. For example, the estimated experimental rate constants in one experiment[36] were about one order greater than the later experimental estimates,[34,35] whereas the theoretical work at the PUMP3/6-

10.1021/jp001324c CCC: $19.00
Published on Web 08/18/2000

311G(d,p)//UHF/6-31G(d) level by Fu et al.[39] supported ref 36. Therefore, it is in great need to perform higher level calculations to test these experimental results.

In this paper, we decide to perform high level ab initio calculations to obtain the electronic structure information on the reactants, products, transition state and some selected points along the minimum energy path, and use the canonical variational transition state theory incorporating a small-curvature tunneling correction method (CVT/SCT) to calculate the rate constants and activation energies in an extremely wide temperature range from 20 to 5000 K. The present obtained barrier height of 2.22 kcal/mol exactly falls in the region 2.0−2.5 kcal/mol by many groups.[17,18,24,28,30] The forward reaction rate constants are in good agreement with most of the available experimental data over a broad temperature region. Also, the obtained rate constants for the reverse reaction of C_2H_2 with H agree well with some experiments[34,35] yet differ from the other experimental estimates[36−38] and one low level ab initio calculation.[39]

2. Computational Methods

The geometries and vibrational frequencies of the stationary points, i.e., reactants, products, and transition state, are calculated at the UQCISD/6-311+G(d,p) level by using the Gaussian 98 program package.[40] At the same level, the minimum energy path (MEP) is obtained by the intrinsic reaction coordinate (IRC) calculations with a gradient step size of 0.05 $(amu)^{1/2}$ bohr. Furthermore, the stationary points and selected points along the MEP are refined by the G2//UQCISD method[41] which applies the G2 calculation at the UQCISD/6-311+G(d,p) geometries and frequencies rather than the UMP2/6-31G(d) geometries and UHF/6-31G(d) frequencies.

By means of the POLYRATE8.0 program,[42] the theoretical rate constants and activation energies are calculated using the conventional transition state theory (TST), canonical variational transition state theory (CVT), and canonical variational transition state incorporating a small-curvature tunneling correction (CVT/SCT) method. Throughout the CVT and CVT/SCT calculations, the reorientation of the dividing surface (RODS) method[43] is employed. The Euler single-step integrator with a step size of 0.0001 $(amu)^{1/2}$ bohr is used to follow the MEP, and the generalized normal-mode analysis is performed every 0.01 $(amu)^{1/2}$ bohr. The curvature components are calculated using a quadratic fit to obtain the derivative of the gradient with respect to the reaction coordinate. Within the temperature range 20−5000 K, the rate constants at some temperature points and the reaction activation energies for several temperature pairs are computed using mass-scaled Cartesian coordinate.

3. Results and Discussions

3.1. Stationary Points. The optimized geometric parameters of the reactants (C_2H and H_2), product (C_2H_2) and transition state at the UQCISD/6-311+G(d,p) level are shown in Figure 1. The optimized bond lengths of the reactants and products are in good agreement with the experimental data.[44−46] The transition state is a planar structure with C_s symmetry. In the transition state structure, the bond $C_{(1)}-H_{(3)}$ is cis with respect to the $C_{(2)}-H_{(4)}$ bond, and the bond $H_{(3)}-H_{(5)}$ is cis with respect to the $C_{(1)}-C_{(2)}$ bond. The angles $\angle C_{(2)}C_{(1)}H_{(3)}$, $\angle H_{(4)}C_{(2)}C_{(1)}$, and $\angle C_{(1)}H_{(3)}H_{(5)}$ are 168.51°, 177.03°, and 179.92°, respectively. The length of $H_{(3)}-H_{(5)}$ bond that will be broken is only 5% larger than the equilibrium bond length of the hydrogen molecule. The length of bond $C_{(1)}-H_{(3)}$ that will be formed is by 50% larger than the equilibrium bond length of acetylene.

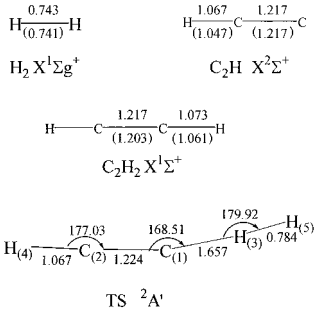

$H_2\ X^1\Sigma g^+$ $C_2H\ X^2\Sigma^+$ $C_2H_2\ X^1\Sigma^+$ TS $^2A'$

Figure 1. Optimized geometric parameters (in angstroms and degrees) of the reactants, product, and transition state at the UQCISD/6-311+G-(d,p) level. The values in the parentheses are the experimental values.[44−46]

TABLE 1: Calculated Harmonic Frequencies (in cm^{-1}) and Zero-Point Energies (ZPE, in kcal/mol) of the Reactants, Product, and Transition State at the UQCISD/6-311+G(d,p) Level

species	frequencies[a]	ZPE[b]
H_2	4422	6.32
C_2H	3479 2038 69(2)	9.23
C_2H_2	3534 3436 2017 771(2) 569(2)	16.68
TS	3480 3350 2030 602 582 471 444 105 679*i*	15.82

[a] The experimental vibrational frequencies are 4355 for H_2;[47] 3372, 3289, 1974, 729(2), 609(2) for C_2H_2;[48] 3298, 1840, 372(2) for C_2H.[49] [b] The frequencies (in cm^{-1}) and the zero-point energy for the transition state at the POL-CI level by Harding et al.[28] are 3367, 2940, 2091, 674, 538, 139, 902*i*, and 15.8 kcal/mol.

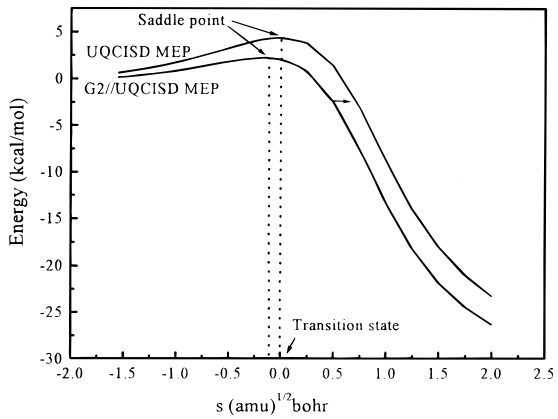

Figure 2. MEP curves at the QCISD/6-311+G(d,p) and G2//QCISD levels.

Therefore, the transition state structure is reactant-like, and the hydrogen abstraction reaction will proceed via an early transition state.

The harmonic vibrational frequencies of the reactants, product, and transition state are listed in Table 1. The maximum error of the calculated frequencies of H_2 and C_2H_2 is 7% compared with the experimental values.[47,48] For the ground state C_2H, the calculated C−H stretching, C−C stretching and C−H bending frequencies are greater than the experimental values[49] by 5.5%, 11% and 26%, respectively. The transition state possesses one and only one imaginary frequency.

Figure 2 shows the minimum energy path (MEP) at the UQCISD and G2//UQCISD levels without ZPE correction. It should be pointed out that the saddle point along the G2//UQCISD MEP does not correspond to the transition structure optimized at the UQCISD/6-311+G(d,p) level. According to the discussion of García et al.,[50] the energy differences between the saddle point at the G2//UQCISD MEP

TABLE 2: Total Energies (in hartree) and Relative Energies (in kcal/mol) of the Reactants, Products, Transition State, and the Saddle Point on G2//QCISD MEP[a]

	UQCISD		G2//UQCISD	
	E + ZPE	$\Delta(E$+ZPE)	E + ZPE	$\Delta(E$+ZPE)
$C_2H + H_2$	−77.558 974 50	0	−77.643 204 0	0
$C_2H_2 + H$	−77.601 924 2	−26.95	−77.689 452 0	−29.01
TS	−77.551 746 9	4.64	−77.639 518 7	2.31
saddle^{G2}	−77.551 716 4	4.55	−77.639 184 7	2.52

[a] The experimental result of the heat of reaction based on the standard heats of formation of the reactants and products are −28.72 kcal/mol.[51]

TABLE 3: Forward and Reverse Barriers at the UQCISD and G2//UQCISD Levels (in kcal/mol)[a]

	UQCISD		G2//UQCISD	
	V_E	V_{E+ZPE}	V_E	V_{E+ZPE}
forward	4.37	4.64	2.22	2.52
reverse	32.45	31.59	32.36	31.53

[a] The forward or reverse barrier at the G2//UQCISD level is the relative energy between reactants or products and the saddle point on the G2//UQCISD MEP.

and the reactants and products at the G2//UQCISD level can be well adopted as the forward and reverse barriers, respectively. In Table 2, we list the total energies (E + ZPE) and relative energies (Δ(E + ZPE)), (set the sum of the total energies of the two reactants calculated independently to be zero of energy) of the reactants, products, transition state, and the saddle point along the G2//UQCISD MEP. In Table 3, we report the forward and reverse barriers at the UQCISD and G2//UQCISD levels. From Table 2, the heat of reaction with ZPE correction at the UQCISD and G2//UQCISD level are −26.95 and −29.01 kcal/mol, respectively, while the experimental heat of reaction, based on the heats of formation of the reactants and products, is −28.72 kcal/mol.[51] The forward and reverse barriers obtained at the UQCISD/6-311+G(d,p) level without ZPE correction are 4.37 and 32.45 kcal/mol, respectively. At the G2//UQCISD level, the forward and reverse barriers without ZPE correction are 2.22 and 32.36 kcal/mol, while with ZPE correction the barriers are 2.52 and 31.53 kcal/mol, respectively. We can see that the forward barrier height of 2.22 kcal/mol without ZPE correction and 2.52 kcal/mol with ZPE correction at the G2//UQCISD level exactly reproduces the value of 2.0−2.5 kcal/mol proposed by many groups.[17,18,24,28,30] Since the forward barrier is far less than the reverse barrier, the forward reaction happens more easily than the reverse reaction.

It should be noted that our bent transition state structure obtained at the UQCISD/6-311+G(d,p) level is different from the linear transition state obtained at the POL-CI level by Harding et al.[28] and at the MP2/6-31G(d,p) level by Kamiya.[29] Although the linear transition state can be reproduced at the MP2/6-31G(d,p) level with only one imaginary frequency, the optimization of transition state under the assumption of a linear geometry leads to a three-imaginary-frequency structure at both the MP2/6-311+G(d,p) and UQCISD/6-311+G(d,p) levels. The three-imaginary -frequency linear structure is only 0.3 kcal/mol over the bent transition state at the QCISD/6-311+G(d,p) level and the energy difference between them is near zero at the G2//QCISD level. At the QCISD/6-311+G(d,p) level, the spin contaminations for both the bent transition state and the linear three-imaginary structure are almost the same, i.e., their $\langle S^2 \rangle$ values are both about 1.17 (0.87 after annihilation) while the normal value is 0.75.

3.2.. Reaction Path Properties. The minimum energy path (MEP) is calculated at the UQCISD/6-311+G(d,p) level by the intrinsic reaction coordinate theory and is further refined by the G2//UQCISD method. As shown in Figure 2, the shapes of the two MEP profiles at the UQCISD and G2//UQCISD levels are very alike but the position of the maximum value along the G2//UQCISD refined MEP is located at about $s = -0.140$ (amu)$^{1/2}$ bohr. On the basis of the G2//UQCISD refined MEP, the classical potential energy $V_{MEP}(s)$ and the adiabatic ground-state potential $V_a^G(s)$ along the MEP as functions of the reaction coordinate s are plotted in Figure 3. The $V_{MEP}(s)$ and $V_a^G(s)$ curves are similar in shape. For a deeper understanding of the variational effect, the dynamic bottleneck properties of the reaction are listed in Table 4. It is shown that the positions s of the variational transition state at various temperatures deviate from the saddle point at $s = 0$. The deviation of s is small at low temperatures and the differences between $V_{MEP}(s)$ and $V_{MEP}(s=0)$, and $V_a^G(s)$ and $V_a^G(s=0)$ are both small. With the increasing of temperature, the deviation of s becomes larger and the maximum deviation at 5000 K is 0.2101 (amu)$^{1/2}$ bohr(amu)$^{1/2}$ bohr, and the corresponding absolute values of $V_{MEP}(s=0.2101) - V_{MEP}(s=0)$ and $V_a^G(s=0.2101) - V_a^G(s=0)$ are 1.17 and 1.64 kcal/mol, respectively. It means that the variational effect is small at low temperatures but should be considered at high temperatures in the calculation of rate constants of this reaction.

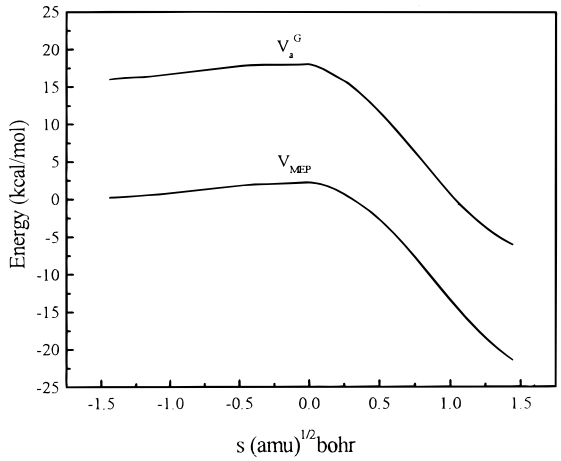

Figure 3. Classical potential energy (V_{MEP}) and ground-state adiabatic potential energy (V_a^G) at the G2//UQCISD level as functions of s (amu)$^{1/2}$ bohr.

TABLE 4: Bottleneck Properties of Reaction (Based on the CVT Method)

T (K)	s (amu)$^{1/2}$ bohr	V_{MEP} (kcal/mol)	V_a^G (kcal/mol)
0	−0.0037	2.22	18.04
20	−0.0036	2.22	18.04
50	−0.0036	2.22	18.04
100	−0.0035	2.22	18.04
150	−0.0034	2.22	18.04
191	−0.0030	2.22	18.04
293	−0.0009	2.22	18.04
325	0.0001	2.22	18.04
500	0.0182	2.18	17.98
854	0.0653	2.03	17.75
1000	0.0808	1.96	17.65
1500	0.1207	1.74	17.35
2000	0.1472	1.56	17.10
3000	0.1793	1.32	16.77
4000	0.1980	1.16	16.56
5000	0.2101	1.05	16.40

Figure 4 shows the bond length changes along reaction coordinate s. It is shown that the bond lengths, $C_{(1)}-H_{(3)}$ and $H_{(3)}-H_{(5)}$, change strongly in the course of reaction. The bond that broke, $H_{(3)}-H_{(5)}$, elongates after $s = -0.5$ (amu)$^{1/2}$ bohr.

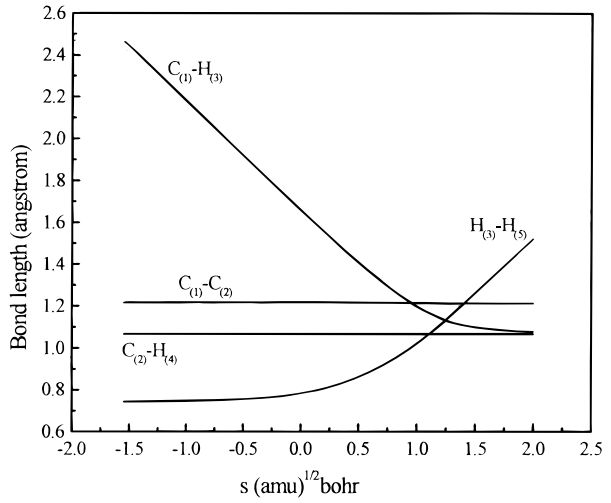

Figure 4. Changes of the bond lengths (in angstroms) as functions of s (amu)$^{1/2}$ bohr at the UQCISD/6-311+G(d,p) level.

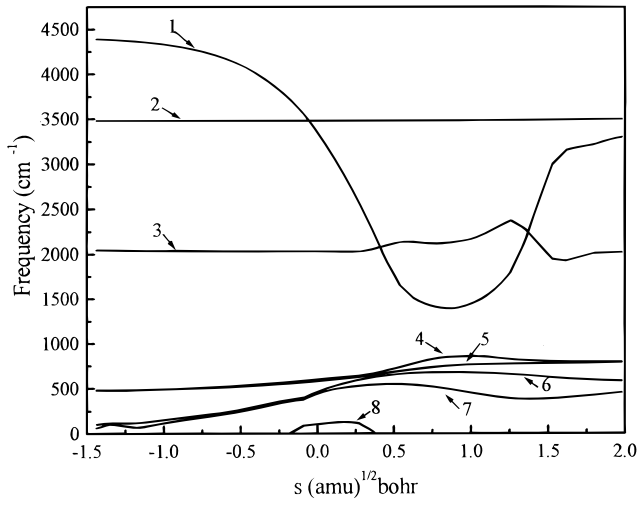

Figure 5. Changes of the generalized normal mode vibrational frequencies as functions of s (amu)$^{1/2}$ bohr at the UQCISD/6-311+G-(d,p) level.

The $C_{(1)}-H_{(3)}$ bond rapidly shortens from reactants side and arrives to the equilibrium bond length of C_2H_2 at about $s = 1.5$ (amu)$^{1/2}$ bohr. It can be seen that the geometric changes mainly take place in the region from about $s = -0.5$ to 1.5 (amu)$^{1/2}$ bohr.

The vibrational frequencies of generalized normal modes are shown in Figure 5 as functions of the reaction coordinate s. In the negative limit of s, the frequencies correspond to those of the reactants, mode (1) to H_2 and modes (2)−(5) to C_2H, and in the positive limit of s, the frequencies are associated with the product, modes (1)−(7) to HCCH. The vibrational frequency of mode (1) changes dramatically in the course of the reaction, corresponding to the $H_{(3)}-H_{(5)}$ stretching of molecule hydrogen at $s = -\infty$ (reactants region), and the $C_{(1)}-H_{(3)}$ stretching in C_2H_2 at $s = +\infty$ (products region). The vibrational transformation from $H_{(3)}-H_{(5)}$ stretching vibration to $C_{(1)}-H_{(3)}$ stretching vibration takes place in the range −0.5 to 1.5 (amu)$^{1/2}$ bohr. Therefore, the mode (1) can be referred to as the "reaction mode". The frequency of mode (2) correlating with the $C_{(2)}-H_{(4)}$ stretching vibration almost remains unchanged, and the frequencies of mode (3) correlating with the $C_{(1)}-C_{(2)}$ stretching vibration has a small fluctuation at 0.25 (amu)$^{1/2}$ bohr $< s <$ 1.75 (amu)$^{1/2}$ bohr. It means that the $H_{(3)}$ abstraction process does not influence the $C_{(2)}$-$H_{(4)}$ stretching vibration but the forming of $C_{(1)}-H_{(3)}$ bond has a little influence on $C_{(1)}-C_{(2)}$ stretching vibration. The modes (4) and (5) are the degenerate bending vibrations with respect to $C_{(1)}-C_{(2)}-H_{(4)}$ on the reactants' side; they transform to degenerate bending modes of acetylene in the course of reaction. The two new bending vibrations of mode (6) and (7) form another degenerate bending modes in the products side. The mode (8) is a binding vibration correlating with the formation of transition state, so it only appears near the transition state region and disappears toward both the directions of the reactants and the products.

3.3. Rate Constants. In the calculation of rate constants, we shift the whole MEP curve at the G2//UQCISD level along the reaction coordinate s so that its maximum energy corresponds to the transition state structure optimized at the UQCISD level ($s = 0$). Sixteen extra points near the transition state region along MEP, eight points in the each side of reactants and products, are selected in the canonical variational transition state theory calculation. The energies of reactants and products are calculated at the G2//UQCISD level, and the energies of the transition state and extra points along reaction path are taken artificially from the shifted G2//UQCISD MEP. For the purpose of comparison, calculations by means of the conventional transition state theory (TST), the canonical variational transition state theory (CVT), and the canonical variational transition state theory with small-curvature tunneling correction (CVT/SCT) are performed for obtaining the reaction rate constants and activation energies for the forward reaction in the temperature range from 20 to 5000 K, and the reverse reaction in the temperature range from 800 to 5000 K. The reorientation of the dividing surface (RODS) method[43] is used in the calculation of rate constants. The RODS method significantly improves low-temperature rate constants.

Table 5 lists our theoretical forward rate constants at the temperatures from 20 to 5000 K together with recent measured experimental results.[6−9,11−13,15,19,22,24,26] For the simplicity of discussion, the TST rate constants, CVT rate constants, CVT/SCT rate constants, and the experimental results of the forward reaction are plotted against the reciprocal of temperature in different temperature ranges, 150 to 1000 K and 2500 to 5000 K, respectively, in Figure 6a,b. The calculated forward rate constants at temperatures lower than 150 K are plotted against temperature in Figure 6c. From Table 5, and Figure 6a−c, we can see that the variational effect and the difference of TST and CVT rate constants are not significant except for very high temperatures. Because of the small-curvature tunneling effect, the CVT/SCT rate constants are greater than the CVT rate constants for temperatures below 500 K, especially at the temperatures below 150 K. For example, the ratios of $k_f^{CVT/SCT}/k_f^{CVT}$ are 1.06 at 500 K, 1.41 at 300 K, 2.51 at 191 K, 5.04 at 150 K, 64 at 100 K, and 4.9×10^6 at 50 K. At very low temperatures, i.e., 20−50 K, the CVT/SCT rate constants are still in the magnitude of 10^{-15} cm^3 molecule^{-1} s^{-1}. It should be noted that the CVT/SCT rate constant decreases to a minimum value of 3.15×10^{-15} at about 50 K, then becomes larger with the decrease of temperature. This conclusion is similar to that of Herbst.[29] He predicted the negative temperature dependence for the forward reaction at temperatures below 40 K.

In comparison of the theoretical result with the experimental values, we limit our discussion to the CVT/SCT rate constants. The CVT/SCT rate constants are in much better agreement with four recent experimental values[18,19,22,24] measured in the temperature range 178−854 K. The rate constant ratio ranges of $k_f^{CVT/SCT}:k_f^{exptl}$ for the four measurements are 0.99−1.07 for

TABLE 5: Forward Reaction Rate Constants (cm^3 $Molecule^{-1}s^{-1}$) for the Temperature Range 20−5000 K

T (K)	TST	CVT	CVT/SCT	exptl
20	8.18×10^{-38}	7.68×10^{-38}	5.10×10^{-15}	
40	1.54×10^{-24}	1.50×10^{-24}	3.29×10^{-15}	
50	6.56×10^{-22}	6.40×10^{-22}	3.15×10^{-15}	
60	3.64×10^{-20}	3.57×10^{-20}	3.26×10^{-15}	
100	1.07×10^{-16}	1.06×10^{-16}	6.78×10^{-15}	
150	5.70×10^{-15}	5.67×10^{-15}	2.86×10^{-14}	
178	2.00×10^{-14}	1.99×10^{-14}	5.90×10^{-14}	$(5.0 \pm 1.1) \times 10^{-14}$ [a]
191	3.17×10^{-14}	3.16×10^{-14}	7.96×10^{-14}	$(5.3 \pm 0.9) \times 10^{-14}$ [a]
213	6.11×10^{-14}	6.09×10^{-14}	1.26×10^{-13}	$(1.1 \pm 0.2) \times 10^{-13}$ [a]
215	6.44×10^{-14}	6.43×10^{-14}	1.30×10^{-13}	$(9.0 \pm 0.3) \times 10^{-14}$ [a]
228	8.91×10^{-14}	8.89×10^{-14}	1.66×10^{-13}	$(2.1 \pm 0.4) \times 10^{-13}$ [a]
293	3.01×10^{-13}	3.01×10^{-13}	4.32×10^{-13}	$(7.1 \pm 1.1) \times 10^{-13}$ [b]
295	3.10×10^{-13}	3.10×10^{-13}	4.42×10^{-13}	4.7×10^{-13} [c]
				$(6.9 \pm 0.7) \times 10^{-13}$ [d]
298	3.24×10^{-13}	3.24×10^{-13}	4.59×10^{-13}	1.5×10^{-13} [e]
				$(4.8 \pm 0.3) \times 10^{-13}$ [f]
				9.7×10^{-13} [g]
300	3.34×10^{-13}	3.34×10^{-13}	4.70×10^{-13}	$(4.6 \pm 0.7) \times 10^{-13}$ [a]
				$(1.2 \pm 0.3) \times 10^{-11}$ [h]
320	4.38×10^{-13}	4.38×10^{-14}	5.89×10^{-13}	1.7×10^{-13} [i]
325	4.67×10^{-13}	4.67×10^{-13}	6.22×10^{-13}	8.7×10^{-13} [d]
344	5.85×10^{-13}	5.85×10^{-13}	7.53×10^{-13}	9×10^{-13} d
355	6.61×10^{-13}	6.61×10^{-13}	8.36×10^{-13}	$(6.7 \pm 0.9) \times 10^{-13}$ [a]
359	6.90×10^{-13}	6.90×10^{-13}	8.67×10^{-13}	$(7.5 \pm 0.8) \times 10^{-13}$ [a]
380	8.52×10^{-13}	8.52×10^{-13}	1.04×10^{-12}	1.06×10^{-12} [d]
412	1.14×10^{-12}	1.14×10^{-12}	1.34×10^{-12}	1.22×10^{-12} [d]
425	1.27×10^{-12}	1.26×10^{-12}	1.46×10^{-12}	1.27×10^{-12} [d]
440	1.42×10^{-12}	1.42×10^{-12}	1.61×10^{-12}	1.41×10^{-12} [d]
466	1.72×10^{-12}	1.71×10^{-12}	1.87×10^{-12}	2.8×10^{-12} [c]
500	2.15×10^{-12}	2.13×10^{-12}	2.25×10^{-12}	
660	4.88×10^{-12}	4.66×10^{-12}	4.41×10^{-12}	7.10×10^{-12} [c]
854	9.72×10^{-12}	8.81×10^{-12}	7.73×10^{-12}	1.27×10^{-11} [c]
1000	1.45×10^{-11}	1.26×10^{-11}	1.07×10^{-11}	
1500	3.85×10^{-11}	3.01×10^{-11}	2.42×10^{-11}	
2000	7.52×10^{-11}	5.46×10^{-11}	4.35×10^{-11}	
2500	1.25×10^{-10}	8.62×10^{-11}	6.91×10^{-11}	
2580	1.34×10^{-10}	9.19×10^{-11}	7.39×10^{-11}	3.29×10^{-10} [j]
3000	1.89×10^{-10}	1.25×10^{-10}	1.01×10^{-10}	3.96×10^{-10} [j]
3500	2.66×10^{-10}	1.71×10^{-10}	1.41×10^{-10}	4.65×10^{-10} [j]
4000	3.58×10^{-10}	2.25×10^{-10}	1.86×10^{-10}	5.25×10^{-10} [j]
4650	4.98×10^{-10}	3.05×10^{-10}	2.58×10^{-10}	5.92×10^{-10} [j]
5000	5.83×10^{-10}	3.54×10^{-10}	3.01×10^{-10}	

[a] Reference 22, values of temperature points, $T = 178-359$ K. [b] Reference 17. [c] Reference 19, values of temperature points, $T = 295-854$ K. [d] Reference 24, values of temperature points, $T = 295-440$ K. [e] Reference 7. [f] Reference 13. [g] Reference 9. [h] Reference 12. [i] Reference 8. [j] Reference 26, values of the Arrhenius expression 7.4×10^{14}-$\exp(-3400/T)$ cm^3 $mole^{-1}$ s^{-1}, $T = 2580-4650$ K.

Koshi et al. (298−438 K),[18] 0.61−0.89 for Farhat et al. (295−854 K),[19] 0.79−1.50 for Opansky et al. (178−359 K),[22] and 0.64−1.15 for Peeters et al. (295−440 K).[24] The CVT/SCT rate constants at the temperature range 2580−4650 K are lower than those but also agree well with the experimental values obtained by Kruse et al.[26] The $k_f^{CVT/SCT}$:k_f^{exptl} ratio is in the range 0.22−0.44, and the CVT/SCT rate constants at higher temperatures are closer to the experimental values. The CVT/SCT rate constant of 4.42×10^{-13} cm^3 $molecule^{-1}$ s^{-1} at 295 K and 4.59×10^{-13} cm^3 $molecule^{-1}$ s^{-1} at 298 K agree very well with the later experimental values of Farhat et al.,[19] Stephens,[13] and Lander,[15] but is about a factor of 2.1 lower than the experimental value of Okabe,[9] and a factor of 3 higher than the experimental values of Langer[6] and Laufer.[7,8] The reason for the lower rate constant of Langer has been judged to be incomplete mixing in their observation zone. The early room-temperature rate constants obtained by Renlund,[11,12] 1.2×10^{-11} $cm^3molecule^{-1}s^{-1}$, is much higher than the CVT/SCT rate constant and those of all the other experiments because of the contribution of the vibrationally and/or electronically excited C_2H radical. There

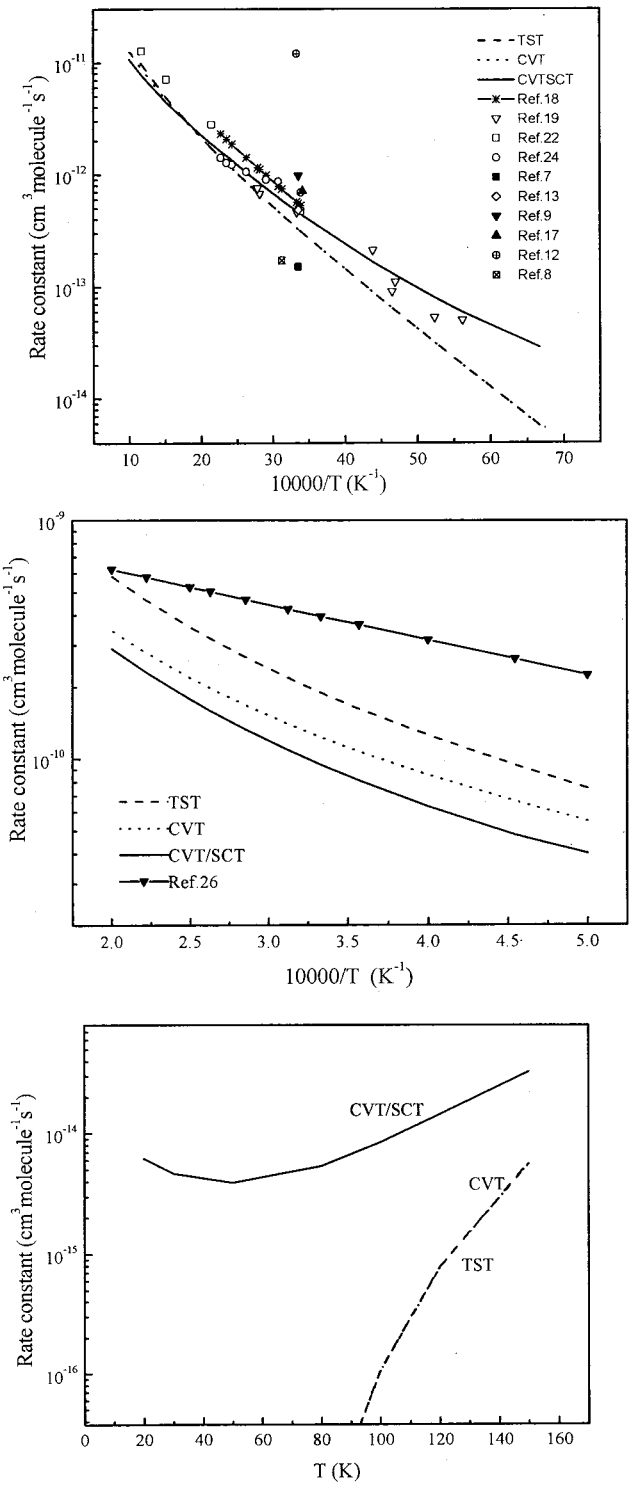

Figure 6. (a) Forward rate constants as functions of the reciprocal of the temperature (K^{-1}) over temperature range150−1000 K. (b) Forward rate constants as functions of the reciprocal of the temperature (K^{-1}) over temperature range 2500−5000K. (c) Forward rate constants k_f (cm^3 $molelecule^{-1}$ s^{-1}) as functions of the temperature (K) over temperature range 20−150K.

are no available experimental rate constants for temperatures below 150 K.

Table 6 lists activation energies based on CVT/SCT method for several two-temperature fits. The activation energy for each temperature fit at the G2//UQCISD level is less than that at the UQCISD level. At both levels, the activation energy gets smaller with the decrease of temperature. In the following discussion, we will adopt all theoretical activation energy values at the G2//

TABLE 6: Activation Energies (kcal/mol) for $C_2H + H_2 \rightarrow C_2H + H$

T range (K)	CVT/SCT (G2)	CVT/SCT (UQCISD)
20−50	−0.032	−0.026
50−100	0.153	0.296
100−150	0.811	1.353
178−359	1.89	2.984
295−440	2.31	3.803
1000−2000	5.57	8.084
2580−4650	14.38	16.754

[a] Activation energies deduced from experimental rate constants expression: 2.16 ± 0.59 kcal/mol (295−440 K),[18] 1.98 ± 0.11kcal/mol (178−359K),[22] 6.76 kcal/mol (2580−4650K).[26]

UQCISD level. At low temperatures, the calculated activation energy values of 1.89 and 2.31 kcal/mol are respectively in good agreement with the experimental activation energies, 1.98 ± 0.11 kcal/mol for the temperature region 178−359 K[22] and 2.16 ± 0.59 kcal/mol for the temperature region 298−438 K,[18] respectively, deduced from the rate constant expression of Opansky et al.[22] and Koishi et al.[18] At high-temperature range 2580−4650 K, we find that the activation energy obtained by CVT/SCT calculation, 14.38 kcal/mol, is much greater than the value of 6.76 kcal/mol deduced from temperature dependence expression of Kruse et al.,[26] although the CVT/SCT rate constants are still in agreement with the experimental values. We think that the temperature dependence of the rate constants at high-temperature region may need careful reinvestigation. At very low-temperature region, the reaction activation energy becomes very small. The predicted activation energy for temperature region 50−100 K is only 0.153 kcal/mol. At temperature range 20−50 K, the activation energy takes a negative value of −0.032 kcal/mol. As a result of negative activation energy at temperatures below 50 K, the CVT/SCT rate constants should be negative temperature dependent.

The calculated reverse reaction rate constants and some reported results at temperatures between 800 and 5000 K are listed in Table 7 and also are plotted as functions of the reciprocal of the temperature in Figure 7. For the reverse reaction, the available literature rate constants are indirect and thus have some uncertainty. From Table 7 and Figure 7, we can see that the CVT/SCT rate constants are in agreement with the recommendations in the two recent evaluations by Baulch et al.,[34,35] but differ from those of some others.[24,36−38] It can also be seen that the variational effect gets greater with the increasing of temperature and should be taken into account at high temperatures while the small-curvature tunneling correction is small for the whole temperature range. Fu et al.[39] have

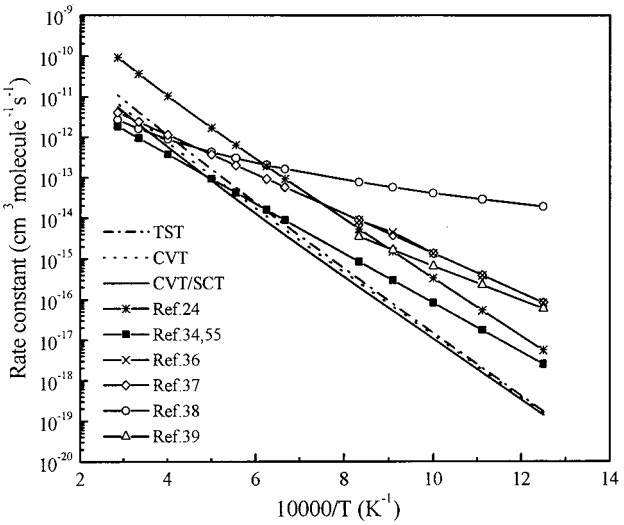

Figure 7. Reverse reaction rate constants k_r (cm^3 molelecule^{-1} s^{-1}) as functions of the reciprocal of the temperature (K^{-1}) over the temperature range 800−5000 K.

reported an ab initio study on the rate constants of the reaction between acetylene and hydrogen atom at the UHF/6-31G(d) level incorporating PUMP3 single-point energy calculation. With a barrier height of 25.56 kcal/mol, their rate constants results for the reverse reaction at 800−1200K are in agreement with the experimental results of Dagaut et al.[36] and Tanzawa et al.[37] but much higher than ours. We think that direct experimental measurement on the reverse rate constants of this reaction is very desirable.

4. Conclusions

The hydrogen abstraction reaction between ethynyl and hydrogen molecule are investigated theoretically. The transition state geometry optimized at the UQCISD/6-311+G(d,p) level is a planar structure and reactant-like. At the G2//UQCISD level, the forward barrier heights without and with zero-point energy correction are obtained to be 2.22 and 2.52 kcal/mol, respectively. The changes of geometry and generalized normal modes mainly take place from about $s = -0.5$ to 1.5 (amu)$^{1/2}$ bohr. The forward CVT/SCT rate constants are in good agreement with most of the experimental results at the temperature range 178−854 K, and also agree well with the experimental result at the temperature range 2580−4650 K. The activation energy of the forward reaction is in agreement with the experimental values at temperature range 178−854 K, but much lower than

TABLE 7: Reverse Rate Constants (in cm^{3}molesule^{-1}s^{-1}) at Temperatures of 800−5000 K

T (K)	TST	CVT	CVT/SCT	ref 24[a]	ref 34,35[b]	ref 36[c]	ref 39[d]
800	1.69×10^{-19}	1.55×10^{-19}	1.38×10^{-19}	5.57×10^{-18}		8.30×10^{-17}	5.89×10^{-17}
900	2.04×10^{-18}	1.83×10^{-18}	1.59×10^{-18}	5.39×10^{-17}		3.94×10^{-16}	2.28×10^{-16}
1000	1.52×10^{-17}	1.32×10^{-17}	1.12×10^{-17}	3.36×10^{-16}	9.15×10^{-17}	1.37×10^{-15}	6.76×10^{-16}
1100	7.92×10^{-17}	6.74×10^{-17}	5.61×10^{-17}	1.52×10^{-15}	3.27×10^{-16}	4.50×10^{-15}	1.66×10^{-15}
1200	3.16×10^{-16}	2.63×10^{-16}	2.16×10^{-16}	5.40×10^{-15}	9.43×10^{-16}	8.83×10^{-15}	3.51×10^{-15}
1500	6.86×10^{-15}	5.36×10^{-15}	4.31×10^{-15}	9.16×10^{-14}	9.73×10^{-15}		
1800	5.52×10^{-14}	4.12×10^{-14}	3.29×10^{-14}	6.32×10^{-13}	4.61×10^{-14}		
2000	1.59×10^{-13}	1.15×10^{-13}	9.20×10^{-14}	1.69×10^{-12}	1.00×10^{-13}		
2500	1.10×10^{-12}	7.60×10^{-13}	6.10×10^{-13}	1.04×10^{-11}	6.34×10^{-13}		
3000	4.16×10^{-12}	2.75×10^{-12}	2.23×10^{-12}	3.65×10^{-11}	1.03×10^{-12}		
3500	1.10×10^{-11}	7.05×10^{-12}	5.79×10^{-12}	9.24×10^{-11}			
4000	2.31×10^{-11}	1.45×10^{-11}	1.21×10^{-11}				
5000	6.82×10^{-11}	4.14×10^{-11}	3.51×10^{-11}				

[a] From rate constants expression $k_r = 1.5 \times 10^{-13} T^{1.32} \exp(-15400/T)$, ref 24. [b] From rate constants expression $k = 1.1 \times 10^{-10} \exp(-14000/T)$ cm^{3}molecule^{-1}s^{-1}, $T = 1000-3000$ K, error limit $\Delta \log k = \pm 1.0$. References 34 and 35. [c] $T = 800-1200$ K, ref 36. [d] CVT/SCSAG rate constants of Fu et al.[39]

the experimental values at temperature range 2580−4650 K. At temperatures below 50 K, the forward CVT/SCT rate constants are found to be negative temperature dependence. The variational effect is small at low temperatures but should be considered at high temperatures. The small-curvature tunneling correction is very important at low temperatures especially at temperatures below 150 K for the forward reaction. For the reverse reaction $C_2H_2 + H \rightarrow C_2H + H_2$ in the temperature range 800−5000 K, the calculated rate constants are in good agreement with two recent recommendations, and the variational effect should be taken into account at high temperatures while the small-curvature tunneling correction takes less importance in the considered temperature range.

Acknowledgment. We thank Professor Donald G. Truhlar for providing the POLYRATE 8.0 program. This work is supported by the National Natural Science Foundation of China (Grant G29892168).

References and Notes

(1) Tucker, K. D.; Kutner, M. L. Thaddeus, P. *Astrophys. J.* **1974**, *193*, L11.
(2) Strobel, D. F. *Planet. Space Sci.* **1982**, *30*, 839.
(3) Shaub, W. M.; Bauer, S. H. *Combust. Flame* **1978**, *32*, 35.
(4) Kiefer, J. H.; Von Drasek, W. A. *Int. J. Chem. Kinet.* **1990**, *22*, 747.
(5) Kruse, T.; Roth, P. *J. Phys. Chem. A* **1997**, *101*, 2138.
(6) Langer, W.; Wagner, H. G. *Ber. Bunsen-Ges. Phys. Chem.* **1975**, *79*, 165.
(7) Laufer, A. H.; Bass, A. M. *J. Phys. Chem.* **1979**, *83*, 310.
(8) Laufer, A. H. *J. Phys. Chem.* **1981**, *85*, 3823.
(9) Okabe, H. *J. Phys. Chem.* **1982**, *78*, 1312.
(10) Laufer, A. H.; Lechleider, R. *J. Phys. Chem.* **1984**, *88*, 66.
(11) Renlund, A. M.; Shokoohi; F.; Reisler, H.; Witting, C. *Chem. Phys. Lett.* **1981**, *84*, 293.
(12) Renlund, A. M.; Shokoohi; F.; Reisler, H. C. *J. Phys. Chem.* **1982**, *86*, 4165.
(13) Stephens, J. W.; Hall, J. L.; Solka, H. Yan, W.-B.; Curl, R. F. Glass, G. P. *J. Phys. Chem.* **1987**, *91*, 5740.
(14) Lander, D. R.; Unfried, K. G.; Stephen, J. W.; Glass, G. P.; Curl, R. F. *J. Phys. Chem.* **1989**, *93*, 4109.
(15) Lander, D. R.; Unifried, K. G.; Glass, G. P.; Curl, R. F. *J. Phys. Chem.* **1990**, *94*, 7759.
(16) Shin, K. S.; Michael, J. V. *J. Phys. Chem.* **1991**, *95*, 5864.
(17) Koshi, M.; Nishida, N.; Matsui, H. *J. Phys. Chem.* **1992**, *96*, 5875.
(18) Koshi, M. Fukuda, K.; Matsui, H. *J. Phys. Chem.* **1992**, *96*, 9839.
(19) Farhat, S. K.; Morter, C. L.; Glass, G. P. *J. Phys. Chem.* **1993**, *97*, 12789.
(20) Opansky, B. J.; Seakins, P. W.; Pedersen, J. O. P.; Leone, S. R. *J. Phys. Chem.* **1993**, *97*, 8583.
(21) Opansky, B. J.; Leone, S. R. *J. Phys. Chem.* **1996**, *100*, 4888.
(22) Opansky, B. J.; Leone, S. R. *J. Phys. Chem.* **1996**, *100*, 19904.
(23) Look, H. V.; Peeters, J. *J. Phys. Chem.* **1995**, *99*, 16284.
(24) Peeters, J.; Look, H. V.; Ceursters, B. *J. Phys. Chem.* **1996**, *100*, 15124.
(25) Hoobler, R. J.; Opansky, B. J.; Leone, S. R. *J. Phys. Chem. A.* **1997**, *101*, 1339.
(26) Kruse, T.; Roth, P. *J. Phys. Chem. A* **1997**, *101*, 2138.
(27) Chastaing, D.; James, P. l.; Sims, I. R.; Smith, I. W. M. *Faraday Discuss* **1998**, *109*, 165.
(28) Harding, L. B.; Schatz, G. C.; Chiles, R. A. *J. Chem. Phys.* **1982**, *76*, 5172.
(29) Kamiya. A private communication used in ref 17.
(30) Herbst, E. *Chem. Phys. Lett.* **1994**, *222*, 297.
(31) Wang, D. S.; Bowman, J. M. *J. Chem. Phys.* **1994**, *101*, 8646.
(32) Sumathi, R.; Peeters, J.; Nguyen, M. T. *Chem. Phys. Lett.* **1998**, *287*, 109.
(33) Sengupta, D.; Peeters, J.; Thonguyen, M. T. *Chem. Phys. Lett.* **1998**, *238*, 91.
(34) Baulch, D. L.; Cobos, C. J.; Cox, R. A.; Esser, C.; Frank, P.; Just, Th.; Kerr, J. A.; Pilling, M. J.; Troe, J.; Walker, R. W. Warnatz, J. *J. Phys. Chem. Ref. Data* **1992**, *21*, 411.
(35) Baulch, D. L.; Obos, C. J.; Cox, R. A.; Frank, P.; Hayman, G.; Just, Th.; Kerr, J. A.; Murrells, T.; Pilling, M. J.; Troe, J. Walker, R. W.; Warnatz *J. Combust. Flame* **1994**, *98*, 59.
(36) Dagaut, P.; Cathonnet, M.; Boettner, J. C. *Int. J. Chem. Kinet.* **1991**, *23*, 437.
(37) Tsang, W.; Hampson, R. F. *J. Phys. Chem. Ref. Data* **1986**, *15*, 1087.
(38) Tanzawa, T.; Gardiner, W. C. *17th Symp. (Int.) Combust.* **1978**, 563.
(39) Fang, D.; Fu, X. *Int. J. Quantum Chem.* **1994**, *49*, 3.
(40) Frisch, M. J.; Trucks, G. W.; Schlegel, H. B.; Scuseria, G. E.; Robb, M. A.; Cheeseman, J. R.; Zakrzewski, V. G.; Montgomery, J. A., Jr.; Stratmann, R. E.; Burant, J. C.; Dapprich, S.; Millam, J. M.; Daniels, A. D.; Kudin, K. N.; Strain, M. C.; Farkas, O.; Tomasi, J.; Barone, V.; Cossi, M.; Cammi, R.; Mennucci, B.; Pomelli, C.; Adamo, C.; Clifford, S.; Ochterski, J.; Petersson, G. A.; Ayala, P. Y.; Cui, Q.; Morokuma, K.; Malick, D. K.; Rabuck, A. D.; Raghavachari, K.; Foresman, J. B.; Cioslowski, J.; Ortiz, J. V.; Stefanov, B. B.; Liu, G.; Liashenko, A.; Piskorz, P.; Komaromi, I.; Gomperts, R.; Martin, R. L.; Fox, D. J.; Keith, T.; Al-Laham, M. A.; Peng, C. Y.; Nanayakkara, A.; Gonzalez, C.; Challacombe, M.; Gill, P. M. W.; Johnson, B. G.; Chen, W.; Wong, M. W.; Andres, J. L.; Head-Gordon, M.; Replogle, E. S.; Pople, J. A. *Gaussian 98*, revision x.x; Gaussian, Inc.: Pittsburgh, PA, 1998.
(41) Durant, J. L., Jr.; Rohlfing, C. M. *J. Chem. Phys*. **1993**, *98*, 8031.
(42) Chuang, Y.-Y.; Corchado, J. C.; Fast, P. L.;Villà, J.; Hu, W.-P.; Liu, Y.-P.; C. Lynch, G. C.; Nguyen, K. A.; Jackels, C. F.; Zhen Gu, M. G.; Rossi, I.; L. Coitiño, E. L.; Steven Clayton, S.; Melissas, V. S. *POLYRATE*, version 8.0, University of Minnesota: St. Paul, 1998.
(43) Willà, J.; Truhlar, D. G. *Theor. Chem. Acc*. **1997**, *97*, 317.
(44) Gray, H. B. In *Chemical Bonds*; Benjamin, W. A.: Menlo Park, CA**, 1973**.
(45) Strey, G.; Mills, I. M. *J. Mol. Spectrosc.* **1976**, *59*, 103.
(46) . Substitution structure obtained by Bogey, M.; Demuynck, C.; Destombes, J. L. *Mol. Phys.* **1989**, *66*, 955.
(47) Levine, Ira N. In *Molecular Spectroscopy*, Wiley: NewYork, 1975.
(48) Temsaman, M. A.; Hennan *J. Chem. Phys.* **1995**, *102(16)*, 6371.
(49) (a) Stephens, J. W.; Yan, W.-B.; Richnow, M. L.; Solka, H.; Curl, R. F. *J. Mol. Struct.* **1988**, *190*, 41. (b) Kanamori, H.; Hirota, E. *J. Chem. Phys.* **1988**, *89*, 3962. (c) Kanamori, H.; Seki, K.; Hirota, E. *J. Chem. Phys.* **1987**, *87*, 73.
(50) García, J. E.; Corchado, J. C. *J. Phys. Chem.* **1995**, *99*, 8613.
(51) Thermochemical data for reactants and products (in kJ/mol) $\Delta H^0_{f,298}$: H_2, 0.0; C_2H, 566.1; C_2H_2, 228.0; H, 217.998 are taken from *J. Phys. Chem. Ref. Data* **1997**, *26*, 1496.